Exponential frequency spectrum and Lorentzian pulses in magnetized plasmas

D. C. Pace,[a] M. Shi, J. E. Maggs, G. J. Morales, and T. A. Carter
Department of Physics and Astronomy, University of California, Los Angeles, Los Angeles, California 90095, USA

(Received 26 August 2008; accepted 22 October 2008; published online 8 December 2008)

Two different experiments involving pressure gradients across the confinement magnetic field in a large plasma column are found to exhibit a broadband turbulence that displays an exponential frequency spectrum for frequencies below the ion cyclotron frequency. The exponential feature has been traced to the presence of solitary pulses having a Lorentzian temporal signature. These pulses arise from nonlinear interactions of drift-Alfvén waves driven by the pressure gradients. In both experiments the width of the pulses is narrowly distributed resulting in exponential spectra with a single characteristic time scale. The temporal width of the pulses is measured to be a fraction of a period of the drift-Alfvén waves. The experiments are performed in the Large Plasma Device (LAPD-U) [W. Gekelman *et al.*, Rev. Sci. Instrum. **62**, 2875 (1991)] operated by the Basic Plasma Science Facility at the University of California, Los Angeles. One experiment involves a controlled, pure electron temperature gradient associated with a microscopic (6 mm gradient length) hot electron temperature filament created by the injection a small electron beam embedded in the center of a large, cold magnetized plasma. The other experiment is a macroscopic (3.5 cm gradient length) limiter-edge experiment in which a density gradient is established by inserting a metallic plate at the edge of the nominal plasma column of the LAPD-U. The temperature filament experiment permits a detailed study of the transition from coherent to turbulent behavior and the concomitant change from classical to anomalous transport. In the limiter experiment the turbulence sampled is always fully developed. The similarity of the results in the two experiments strongly suggests a universal feature of pressure-gradient driven turbulence in magnetized plasmas that results in nondiffusive cross-field transport. This may explain previous observations in helical confinement devices, research tokamaks, and arc plasmas. © *2008 American Institute of Physics*.
[DOI: 10.1063/1.3023155]

I. INTRODUCTION

The identification of the physical processes underlying low frequency turbulence in magnetized plasmas is a challenging topic in contemporary plasma science.[1] By low frequency it is meant that the characteristic frequency of the fluctuating quantities, ω, is smaller than the ion cyclotron frequency Ω_i. Significant interest in this topic arises from magnetic fusion research because turbulent fluctuations can enhance the transport of mass and energy[2] and thus degrade the performance of confinement devices that aim to achieve fusion conditions. The topic is also of interest in space plasma investigations[3] in which enhanced transport across naturally existing sharp boundaries (in temperature, density, magnetic field) can lead to major effects observable by spacecraft and ground-based instruments.

Significant experimental and theoretical effort has been devoted to the identification of universal trends in the spatial and temporal spectra of turbulent fluctuations in laboratory[4–12] and space plasmas.[13–17] The cited references are just a representative sample of the extensive literature on the subject. The early work by Kolmogorov[18] has had a major influence in these activities.[19] In particular, since, in that pioneering work, a general prediction is made of algebraic spectral dependencies, the published experimental plasma studies typically choose to display the relevant data in a log-log scale. Often, piecewise fits are made to extract power-law indices that are compared to the Kolmogorov prediction. Because of the large dynamic range compressed in log-log displays of data, important phenomena underlying the turbulence can be obscured. That is the situation addressed in this manuscript, in which an exponential frequency dependence is highlighted.

This manuscript reports the results of two different experiments involving pressure gradients across the confinement magnetic field in a large plasma column. Some of the observations were highlighted in Ref. 20 and are expanded in detail in the present manuscript which also includes new modeling features. The two experiments are performed in the Large Plasma Device (LAPD-U) (Ref. 21) operated by the Basic Plasma Science Facility at the University of California, Los Angeles (UCLA). One experiment involves a controlled, pure electron temperature gradient associated with a microscopic hot-electron temperature filament created by the injection of a small electron beam embedded in the center of a large, cold magnetized plasma. The other experiment is a macroscopic limiter-edge experiment in which a density gradient is established by inserting a metallic plate at the edge of the nominal plasma column of the LAPD-U. The tempera-

[a]Electronic mail: pace@physics.ucla.edu.

ture filament experiment permits a detailed study of the transition from coherent to turbulent behavior and the concomitant change from classical to anomalous transport. In the limiter experiment the turbulence sampled is always fully developed and the transport is not classical.

Both experiments exhibit a state of complex behavior characterized by a broadband frequency spectrum that is exponential in nature for frequencies below the ion cyclotron frequency. By carefully examining the individual time series of the fluctuating quantities, the exponential feature has been traced to the presence of pulses having a Lorentzian temporal signature. The Lorentzian pulses arise from nonlinear interactions of drift-Alfvén waves driven by the pressure gradients. In both experiments the temporal width of the pulses is narrowly distributed and is measured to be a fraction of a period of the drift-Alfvén waves. The narrow pulse width sets the single scaling frequency for the observed exponential spectrum. Figure 17 and its accompanying text highlight the necessity of a narrow distribution in pulse width leading to an exponential spectrum. A remarkable consequence of this is the ability to discern the typical time width of individual pulses based on the exponential decay characteristic of the broadband power spectrum.

Exponential frequency spectra have previously appeared in a wide range of published studies but little or no attention has been devoted to their significance. Figure 1(a) of Ref. 22 exhibits exponential behavior over four orders of magnitude in an experiment in a helical confinement device in which proof of inverse cascade has been reported. Figure 1 of Ref. 23 displays exponential dependence in an experiment in a tokamak in which it is claimed that magnetic-fluctuation-induced heat transport is observed. Figure 6(b) in Ref. 24 shows coherent modes embedded in an exponential spectrum in a nonlinear dynamics experiment in a low-pressure arc plasma. Figure 7 of Ref. 25 identifies an exponential spectrum in the magnetic fluctuations at the nominal free-edge of the linear device in which the present studies are performed. These are some concrete examples and should not be considered an exhaustive list of results scattered in the plasma science literature. They were chosen because in these publications the spectra are displayed in a semilog format, making the identification of the exponential feature straightforward for the reader.

The similarity of the results in the two different experiments reported here strongly suggests a universal feature of pressure-gradient driven turbulence in magnetized plasmas that results in nondiffusive cross-field transport. The universal feature is temporal structures consisting of Lorentzian pulses narrowly distributed in width. This finding may explain the origin of the previously cited observations of an exponential spectrum in helical confinement devices, research tokamaks, and arc plasmas. It may also contribute to the understanding of "blob" phenomena[26] and anomalous transport in edge plasmas.[27–30]

The manuscript is organized as follows: Section II provides a general description of the LAPD-U device. It also explains the detailed arrangements for the temperature gradient experiment and the limiter-edge experiment. Section III reports on the temporal evolution of the controlled electron temperature filament. It examines the transition from a quiescent, classical-transport stage to a regime of broadband turbulence with a characteristic exponential frequency spectrum. Section IV reports on the observation of an exponential frequency spectrum in the limiter-edge experiment. In Sec. V the origin of the exponential spectra observed in the two experiments is traced to temporal pulses of Lorentzian shape. Section VI discusses a numerical model of the exponential spectra measured and establishes a relationship between pulse width and the characteristic exponential frequency scale. The sensitivity to distortions of the Lorentzian shape is examined. Conclusions are presented in Sec. VII.

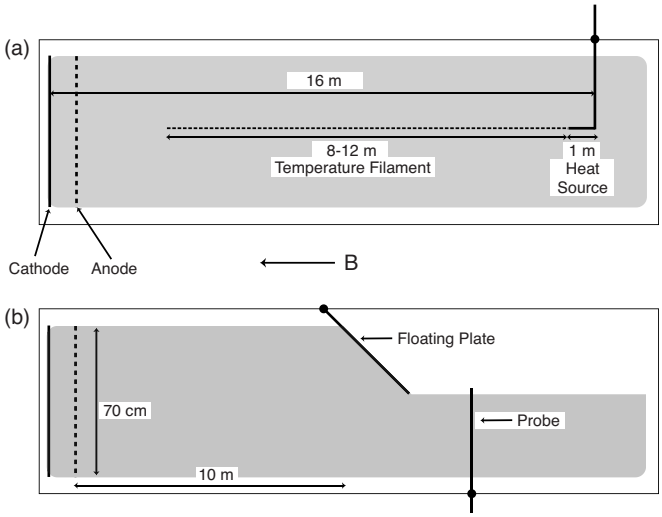

FIG. 1. Schematics of the LAPD-U for the two experimental configurations reported. (a) Temperature gradient experiment. (b) Limiter-edge experiment.

II. EXPERIMENTAL ARRANGEMENT

The experiments reported here are performed in plasmas generated in the upgraded Large Plasma Device (LAPD-U) operated by the Basic Plasma Science Facility at the University of California, Los Angeles (UCLA). A schematic of the device is shown in Fig. 1 for the two different configurations investigated.

The LAPD-U vacuum chamber is 22 m in overall length. Two end-bells (1.5 m diameter, 2 m long) house the turbomolecular vacuum pumps. The plasma section of the device where the experiments are performed is a 1 m diameter vacuum vessel surrounded by water-cooled magnetic coils that provide the radial plasma confinement. The coils are divided into ten groups powered by separate, regulated dc supplies that are computer controlled. Presently this configuration permits practical operation of plasma conditions over the range of 300–2000 G. This arrangement also allows for a wide variety of confinement magnetic-field profiles (e.g., local mirrors or cusps). For the studies reported here the confinement magnetic field is of uniform strength within the magnetic solenoid having a total length of 17.5 m. The plasma is produced by a hot-cathode source located at one end of the main magnetized plasma column. The cathode is a pure nickel sheet coated with a thin layer of barium oxide heated to an emission temperature of about 800 °C. The an-

ode is a molybdenum mesh (approximately 50% transparent) located a distance of 55 cm from the cathode. This source is used to create a pulsed beam of electrons of typical energy in the 50 eV range and carrying currents of 3–6 kA. The energetic electrons (i.e., primaries) that pass through the mesh anode ionize an initial column of neutral He gas (at a fill pressure of $1-2\times10^{-4}$ Torr). Under steady conditions He plasmas having densities in the range of $1-3\times10^{12}$ cm^{-3} are generated with greater than 50% degree of ionization. The characteristic electron temperature is 6 eV with the ion temperature in the range of 1 eV. Plasma pulses several milliseconds in duration are repeated at a 1 Hz rate with a high degree of reproducibility.

For the electron temperature gradient studies sketched in Fig. 1(a), a hot electron channel is established by injecting a small electron beam into the afterglow phase of the plasma, 0.5 ms after the main discharge voltage pulse applied to the cathode is turned-off. The beam is injected at the far end of the machine, 16 m from the cathode, and is directed towards the cathode. The small beam injector is placed at the center of the nominal plasma column whose diameter is 70 cm. During the main discharge the electron temperature is T_e =6 eV, but at the time of beam injection it decays to about 1 eV due to electron heat conduction to the ends of the device, while the plasma density decays on a slow time scale of about 2 ms due to ambipolar flow. The electron beam is 3 mm in diameter and emits a peak current of 250 mA. It is produced by biasing a heated, single crystal of lanthanum–hexaboride (LaB_6) to 20 V relative to the mesh anode of the device. For the relatively low beam voltage used, the additional ionization produced by the beam electrons is negligible. Heat conduction parallel to the magnetic field results in a hot channel approximately 8 m in length and 5 mm in radial extent, with a peak T_e of about 5 eV. The system approximates a nearly ideal situation consisting of a pure electron temperature gradient (i.e., having uniform plasma density) across the magnetic field and embedded in an infinite, colder plasma. Thus, in this case, the observed turbulence and associated transport is insensitive to boundaries.

The limiter-edge experiment utilizes a built-in capability that permits the length of the plasma column in the LAPD-U to be reduced. The length reduction can be achieved by closing a hinged, electrically floating aluminum plate located 10 m from the cathode. In the plasma-edge experiments reported here, this plate is partially closed and used to limit the radial extent of the plasma column on one side, as is sketched in Fig. 1(b). With the plate partially closed, flow of plasma along the magnetic field lines that intersect the plate is terminated at the plate surface. Thus, the plate casts a plasma shadow on the side away from cathode source. In this shadow region a sharp gradient in plasma density is established across the magnetic field. In this study the spectral features of the turbulence associated with this density gradient are investigated and are compared to those found in the controlled temperature filament. The measurements for the limiter-edge experiment are performed during the steady-state stage of the plasma discharge when an accelerating voltage is being applied to the cathode.

III. TEMPERATURE FILAMENT EXPERIMENT

The narrow dimensions of the temperature filament require the use of small, single-tip Langmuir probes for fluctuation and profile measurements in order to achieve millimeter, or better, resolution. In cases where a multiple tip probe is used, the probe tips are laser cut to ensure equivalent collection areas. While some measurements are made with triple probes or through the use of a swept bias to obtain the I-V characteristic, most measurements are of ion saturation current using single-tip probes (or double-sided, single-tip probes). It has been previously shown that the uniform background density of the afterglow plasma permits accurate determination of electron temperature profiles directly from the ion saturation current (I_{sat}) measurements.[31] Two-dimensional profiles, at a fixed axial distance from the heat source, are obtained by computing ensemble averages over twenty discharges at every probe position. This results in thousands of records over a two-dimensional plane, further providing meaningful statistics for turbulence and spectral studies.

The heat supplied to the large plasma column of the LAPD-U by the primary electrons disappears when the accelerating pulse applied to the cathode source is turned off. Consequently, the electron temperature decays due to parallel heat conduction to the ends of the device. At a time of 0.5 ms after the temperature starts to decay the small electron beam described in Sec. II is fired. For the voltage applied, and the parameters of this afterglow plasma, the beam electrons slow down by Coulomb collisions within one meter of the injection point, as is sketched in Fig. 1(a). This region provides a heat source for the colder, afterglow plasma downstream from it. As a consequence of simultaneous axial and transverse heat transport, a temperature filament is generated whose length is approximately 8 m and its radius is a few mm.

The temporal evolution of the temperature filament exhibits three stages, as illustrated by Fig. 2. The solid black curve in Fig. 2 corresponds to the electron temperature measured, using a small triple probe, at an axial distance 384 cm from the beam injector at the radial center of the filament. For this and subsequent figures in this section the strength of the confinement magnetic field is 900 G.

The injected beam current is represented in Fig. 2 by the dotted blue curve, with $t=0$ corresponding to the time when beam injection starts. The dashed red curve shows the decay of the electron temperature in the absence of beam injection, i.e., during the afterglow. It is seen that the heat source supplied by the beam causes a significant increase in temperature. For an interval of about 2 ms after beam injection a quiescent temperature evolution is observed. This behavior corresponds quantitatively to that predicted by the classical theory of heat transport based on Coulomb collisions,[32,33] as has been documented extensively in previous work.[31,34] A second stage can be identified approximately 2 ms after beam injection when high-frequency oscillations become apparent in the electron temperature. These oscillations correspond to coherent drift-Alfvén waves driven unstable by the electron temperature gradient[35] and have been described in

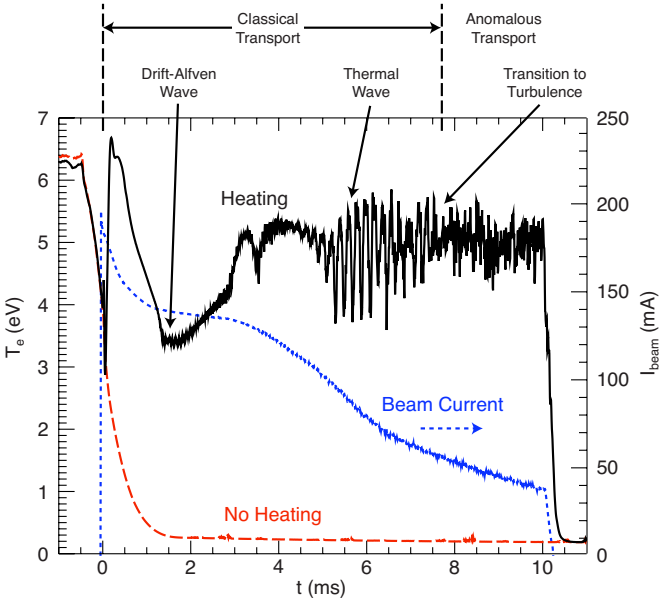

FIG. 2. (Color online) Temporal evolution of the electron temperature at the center of the temperature filament with (solid black) and without (dashed red) heating by the electron beam. Dotted blue curve is the injected beam current.

detail in a previous publication.[36] A third stage appears after 5 ms of beam injection. At this later time low-frequency oscillations mixed with incoherent high-frequency oscillations are observed. This manuscript focuses on the broadband turbulence that arises during this late stage.

Figure 3 illustrates the radial temperature profile of the filament at an axial position $z=384$ cm from the beam injector before the appearance of broadband turbulence. Panel (a) shows a line-cut of T_e through the filament center at a time $t=3$ ms (second stage). Panel (b) displays a two-dimensional, color contour of I_{sat} at $t=1.0$ ms; it demonstrates that the filament is nearly azimuthally symmetric. The solid black curve in panel (a) is the experimental measure-

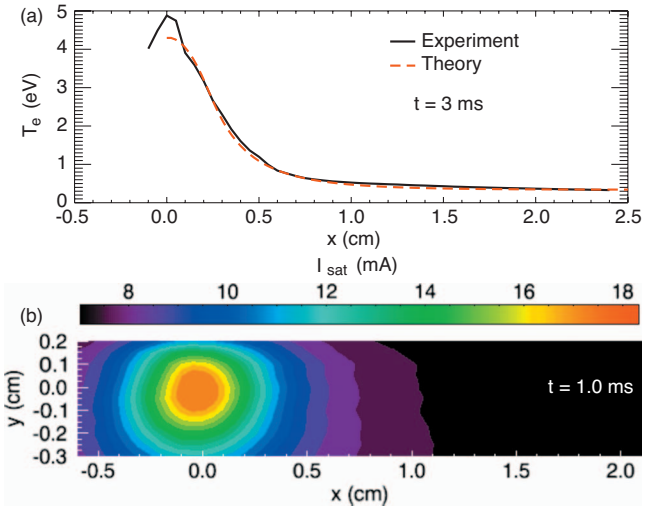

FIG. 3. (Color) Spatial dependence of temperature filament. (a) Black curve is the measured value and the dashed red curve is the prediction from classical theory of transport. (b) Two-dimensional contour of ion saturation current illustrating the symmetry of the filament during early times.

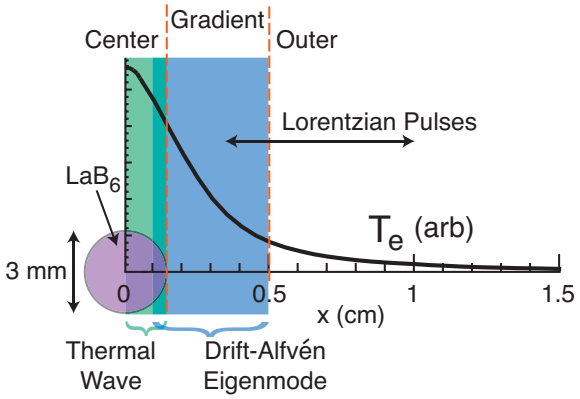

FIG. 4. (Color) Diagram of spatial behavior of fluctuations in the temperature filament experiment. A thermal wave is observed in the center region, the amplitude of the drift-Alfvén waves peaks in the gradient region, and positive Lorentzian pulses are found predominantly in the outer region.

ment while the dashed red curve corresponds to the predictions of a two-dimensional, time-dependent transport code[31] based on Coulomb collisions. It is seen that during this early stage the temperature filament follows closely the classical transport behavior. It is noteworthy that during the second stage coherent drift-Alfvén waves are present but do not cause a significant departure from classical heat transport.

Figure 4 helps in visualizing the different spatial regions that are involved in the turbulent evolution of the temperature filament. In this diagram the continuous solid curve, analogous to those in panel (a) of Fig. 3, shows the radial variation of the electron temperature. The purple circle centered at $r=0$ cm corresponds to the size of the crystal beam source. The region shaded in green ($0.0 \leqslant x \leqslant 1.5$ mm) is what is considered to be the "center region" of the temperature filament. It has the largest temperature and the smallest temperature gradient. It is in this region where low frequency oscillations corresponding to thermal waves[37] are localized. These are the low frequency oscillations that appear at the start of the third stage, close to $t=5$ ms in the Fig. 2 display. The largest temperature gradient is achieved at a radial position about 3 mm from the center of the beam injector. The radial eigenfunction[35,36] of the high-frequency oscillations (i.e., the drift-Alfvén waves) peaks near this location. Accordingly, in Fig. 4 the sector shaded in blue ($1 \leqslant x \leqslant 5$) mm represents the "gradient region" where large $\vec{E} \times \vec{B}$ drifts are expected to arise due to the unstable waves driven by the radial pressure gradient. Finally, for radial distances beyond the gradient region the eigenfunction of the drift-Alfvén waves exhibits a spatial decay. Here the temperature and the temperature gradient are both small. This region is viewed as the "outer region" of the temperature filament. In Fig. 4 the black horizontal line with two opposing arrowheads delineates the spatial domain over which Lorentzian pulses are observed during the third stage of development, i.e., $t>7$ ms in Fig. 2.

Figure 5 provides a useful summary of the individual characteristics of the low-frequency, thermal waves, and of the high-frequency, drift-Alfvén waves. The temporal stage sampled overlaps between the second and third stages iden-

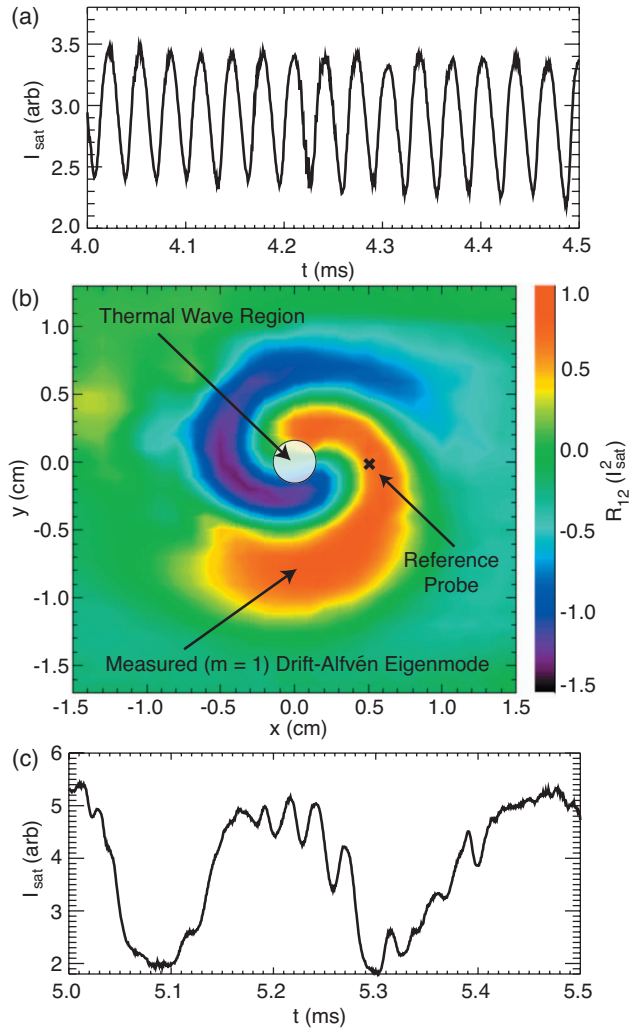

FIG. 5. (Color) Oscillations in ion saturation current due to (a) coherent drift-Alfvén mode and (c) thermal wave. (b) Two-dimensional contour of the cross-covariance, R_{12}, between two probes with axial separation $\Delta z = 160$ cm.

tified in Fig. 2, before the broadband develops. The center panel is a two-dimensional (across the magnetic field) spatial domain that covers the three spatial regions sketched in Fig. 4. The color contour represents the cross-covariance between I_{sat} signals from Langmuir probes separated by an axial distance of $\Delta z = 160$ cm. One probe is fixed at a position $z = 384$ cm away from the beam injector and at a radial position within the region of measurable drift-Alfvén wave activity. The other probe is placed at $z = 544$ cm and it scans a two-dimensional plane across the confinement magnetic field. Measured signals are bandpass filtered to isolate oscillations due to the drift-Alfvén modes. The cross-covariance is calculated for each plasma discharge over a restricted time interval that captures the largest drift-Alfvén wave. The resulting signal is averaged over 20 independent discharge pulses at every spatial location sampled. The result is an amplitude-dependent measurement of the phase difference between the signals of the two probes and contains an imprint of the structure of the coherent drift-Alfvén wave. The light circular region at the center of the drift-Alfvén wave depicts the highly localized thermal oscillation. The trace in

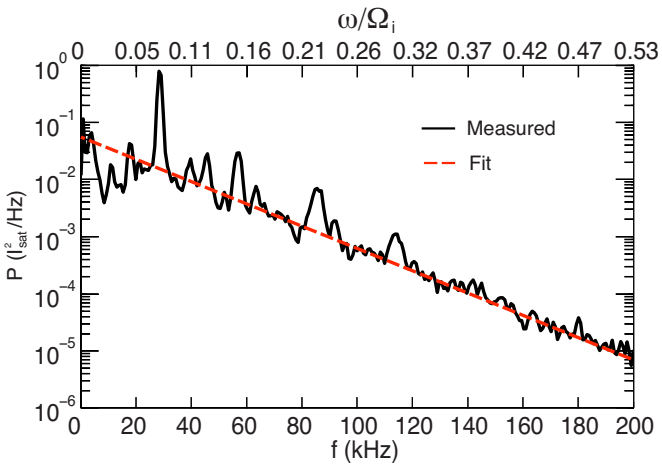

FIG. 6. (Color online) Semilog display of ensemble-averaged power spectrum of fluctuations in ion saturation current in the gradient region of the electron temperature filament. Large peaks corresponding to the coherent drift-Alfvén mode and its harmonics are embedded in a baseline exponential spectrum highlighted by the dashed red line.

the top panel of Fig. 5 shows the time evolution of the ion saturation current at a location $r = 5$ mm, i.e., within the gradient region. It shows the coherent oscillations associated with the two-dimensional snapshot seen in the center panel. These oscillations have typical frequencies in the range of 25–40 kHz. The bottom panel shows the temporal evolution of the ion saturation current at the center of the filament. It is clear that the oscillations here have much lower frequency (by a factor of 5–8) than those in the gradient region. A cross-modulation that shows the faint presence of the drift-Alfvén mode can be seen in portions of the trace.

Next, the spectral features of the third stage of temporal evolution are examined. In this stage the coherent features shown in Fig. 5 are modified. In addition to the narrow spectral peaks associated with the well-separated, thermal oscillations (5 kHz) and the drift-Alfvén waves (25–40 kHz), a broadband spectrum emerges. The characteristic spectrum of fluctuations in the ion saturation current measured in this turbulent stage is shown in Fig. 6. More precisely, the spectrum shown is an ensemble average of individual spectra measured in 20 independent plasma pulses. The bottom scale shows the actual numerical value of the frequency while the top scale shows the more meaningful quantity, namely the frequency scaled to the ion cyclotron frequency. The frequency range covers the fluctuations up to 1/2 of the ion cyclotron frequency. The solid black curve corresponds to the measurement and the dashed red line is a straight line fit to the baseline from which narrow peaks protrude. The narrow peaks correspond to the modes shown in Fig. 5 and their harmonics. The issue of interest here is the nature of the broadband within which the narrow peaks are embedded. Since Fig. 6 is a semilog display, the significance of the straight, dashed red line is that the broadband exhibits an exponential frequency dependence, i.e., the broadband spectrum has the functional form

$$S(\omega) = S_o \exp(-\omega/\omega_s), \tag{1}$$

where S_o is the amplitude and ω_s is a scaling frequency.

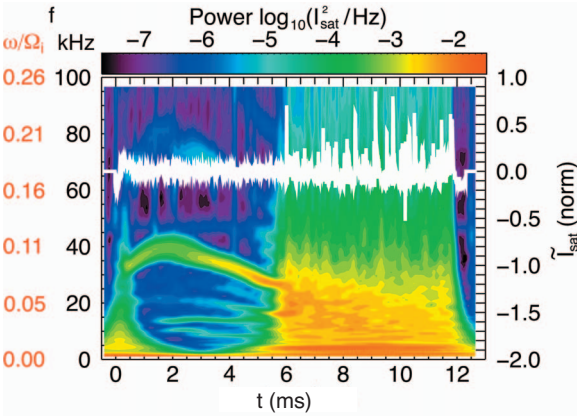

FIG. 7. (Color) Time evolution of power spectrum (color contour) of fluctuations in ion saturation current for the temperature filament experiment. A transition from a classical transport regime with coherent oscillations to a state of enhanced transport and broadband fluctuation spectrum is seen at $t \approx 5.5$ ms. This transition corresponds to the appearance of Lorentzian pulses in the single-shot time series (solid white).

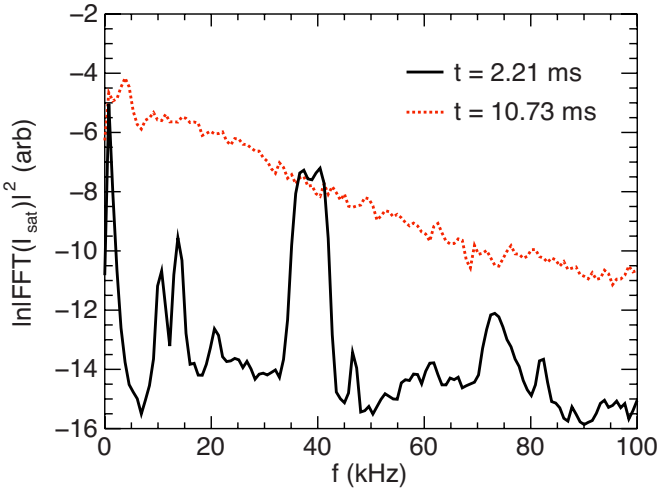

FIG. 8. (Color online) Semilog display of spectrum extracted at selected intervals from the color contour presentation of Fig. 7. Times indicate the center of the FFT window used to calculate the power spectrum. For the early time of 2.21 ms (solid black curve) coherent drift-Alfvén wave peaks are clearly visible. At the later time of 10.73 ms (dotted red curve), after the transition to broadband turbulence has occurred, an exponential spectrum overwhelms the coherent peaks.

Evidence for a link between the broadband spectrum, the interaction of low-frequency oscillations with drift-Alfvén waves, and the generation of pulses is summarized in Fig. 7. The color display corresponds to the time evolution of the ion saturation current (I_{sat}) power spectrum calculated using a continuous wavelet transform (CWT) method at a radial position 9 mm from the filament center (outer region in Fig. 4). The single white trace at the top of Fig. 7 is the fluctuating part of the ion saturation current (normalized to the nonfluctuating part) for one of the 20 plasma discharges that make up the ensemble used to calculate the power spectrum. In the time interval $t < 5.5$ ms the spectrum shows a temporally evolving, coherent drift-Alfvén mode at a frequency between 25–40 kHz and no broadband noise. At these earlier times classical transport due to Coulomb collisions is observed. But at about $t = 5.5$ ms, positive pulses are seen to arise. Departure from classical transport, as previously documented by Burke *et al.* in Fig. 18 of Ref. 36, is observed to occur simultaneously with the appearance of exponential power spectra of the type shown in Fig. 6. Simultaneously, with the generation of the pulses, it is seen that a strong low-frequency (close to 5 kHz) modulation appears and the coherent drift-Alfvén mode disappears into a broadband spectrum.

A striking display of the transition in the character of the fluctuation spectrum is seen in Fig. 8. The quantity displayed in semilog form is the spectral power of the fluctuations in the ion saturation current. The two curves shown correspond to line cuts through the evolving spectrum displayed as a color contour in Fig. 7. The solid black curve is the spectrum at $t = 2.21$ ms (second stage of Fig. 2) and the dotted red line is the spectrum at $t = 10.73$ ms (late into the third stage). It is seen that early in time there is no exponential feature in the fluctuation spectrum. What is observed are peaks corresponding to drift-Alfvén modes and their harmonics. But late in time these peaks are overwhelmed by the appearance of the exponential spectrum.

Figure 9 illustrates the presence of an enhanced, or anomalous, transport regime. This is evident from the difference in radial extent between the measured electron temperature profile (solid black curve) and the classical model profile (dashed red curve). As seen in Fig. 2, the electron temperature maintains a nearly constant peak value during the latter half of beam heating. During this time, however, the temperature profile widens beyond that expected from a system described by classical transport. The transition to anomalous transport is accompanied by the appearance of Lorentzian pulses.

IV. LIMITER-EDGE EXPERIMENT

As described in Sec. II, the environment of the limiter-edge experiment differs significantly from that of the temperature filament. But what they share in common is the

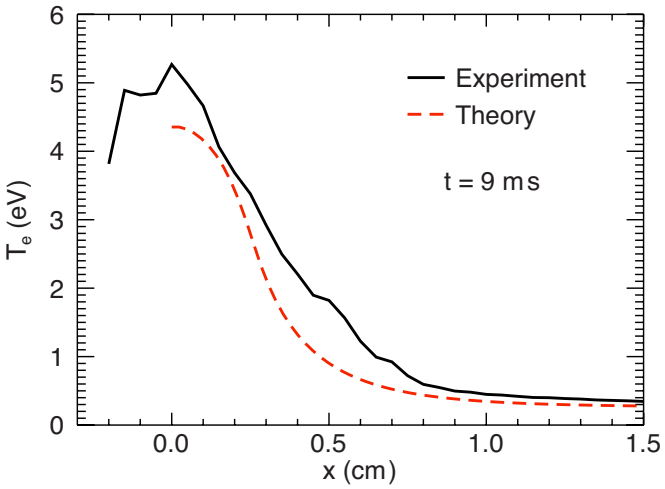

FIG. 9. (Color online) Radial profile of the electron temperature in the turbulent regime. Solid black curve is a measurement and the dashed red curve is a prediction of the classical theory of transport.

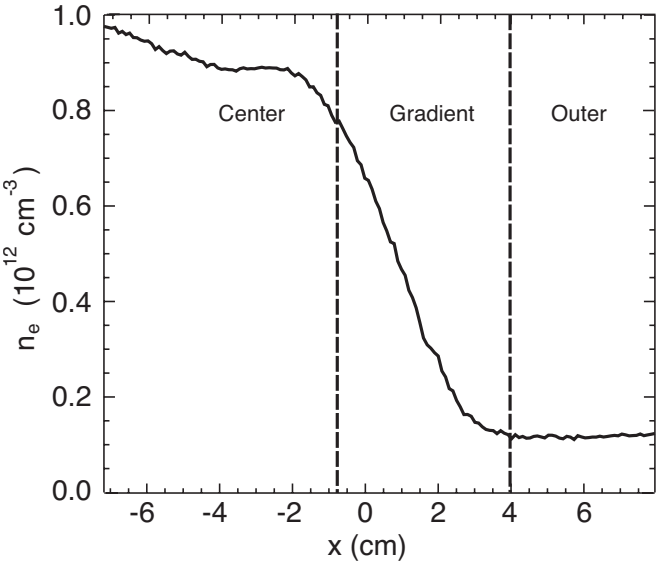

FIG. 10. Density profile of the limiter-edge experiment. The vertical dashed lines separate three distinct regions of behavior equivalent to the center, gradient, and outer regions highlighted for the temperature filament experiment in Fig. 4.

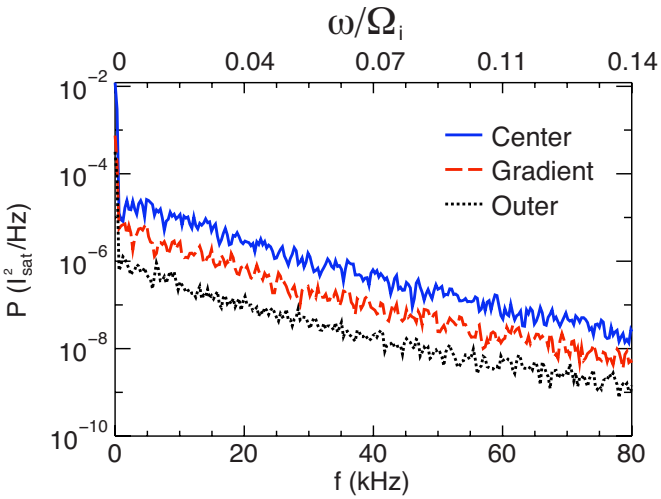

FIG. 11. (Color online) Semilog display of ensemble-averaged power spectra of fluctuations in ion saturation current from the limiter-edge experiment exhibits an exponential frequency dependence in all the spatial regions. To be compared to Fig. 6.

presence of a pressure gradient across the confinement magnetic field. In the temperature filament the pressure gradient is associated with a pure temperature gradient, while in the limiter-edge experiment the pressure gradient arises predominantly from a plasma density gradient. The temperature filament can be considered to be a microscopic structure with a characteristic temperature gradient length, $L_T = T_e/|\nabla T_e| = 0.63$ cm, while the limiter-edge experiment samples a macroscopic region with a characteristic density gradient length, $L_n = n/|\nabla n| = 3.46$ cm. The temperature filament is essentially surrounded by an infinite, cold plasma of significant density. In contrast the limiter-edge comes in contact with neutral gas and a nearby metallic wall.

Figure 10 displays the spatial dependence of the time-averaged ion saturation current across the magnetic field for the limiter-edge configuration. The strength of the confinement magnetic field is 1.5 kG for all the limiter-edge results reported here. Following the spatial classification introduced in Fig. 4 for the temperature filament, in this case a "center region," a "gradient region" and an "outer region" can also be identified, as indicated by the labels in Fig. 10.

In contrast to the temperature filament experiment, the fluctuations in the limiter-edge experiment are always sampled in a broadband turbulent state. This results because the limiter-edge situation does not have a well-defined starting time, akin to the beam turn-on. The behavior is analogous to the third stage in the temporal development of the temperature filament. Accordingly, in the edge study it is not possible to generate a figure corresponding to Fig. 7 in which a clear transition from coherent modes to broadband turbulence is identified. Thus one must examine the shape of the fluctuation spectrum of the turbulent state.

Figure 11 is a semilog display of the ensemble-averaged spectrum of fluctuations in the ion saturation current. The three curves displayed correspond to the spectrum measured in the three spatial regions of the edge density profile identified in Fig. 10. Remarkably, it is found that the turbulence at the plasma edge exhibits a clear exponential frequency dependence, as demonstrated by the three straight lines seen in the semilog display. This finding and the results of the temperature filament strongly suggest that an exponential frequency spectrum is a universal feature of pressure gradient-driven turbulence in magnetized plasmas.

Next, the connection of the exponential spectrum to Lorentzian pulses is investigated.

V. LORENTZIAN PULSES

A normalized, temporal Lorentzian pulse centered at time t_o and having width τ has the mathematical form

$$g(t) = \tau^2[(t - t_o)^2 + \tau^2]^{-1}, \tag{2}$$

and a corresponding Fourier transform

$$\tilde{g}(\omega) = \pi\tau \exp(-\omega\tau + i\omega t_o), \tag{3}$$

whose amplitude has an exponential frequency dependence. This correspondence suggests that the broadband turbulence measured in the temperature filament and at the limiter-edge may contain structures that exhibit a Lorentzian temporal signature.

To identify individual pulses, it is necessary to examine the behavior of the time series measured for a single plasma discharge, since an ensemble average of the traces would lead to a strong cancellation of these features. A difficulty in extracting "pulse events" from the measurement of ion saturation current in the temperature filament experiment is that such signals also contain oscillatory behavior related to the coherent thermal mode and the drift-Alfvén waves. To overcome this difficulty, in this investigation a variety of pulse extraction techniques have been used. The various methods have consistently led to the identification of temporally localized pulses having Lorentzian shape under conditions that simultaneously register an ensemble-averaged, broadband

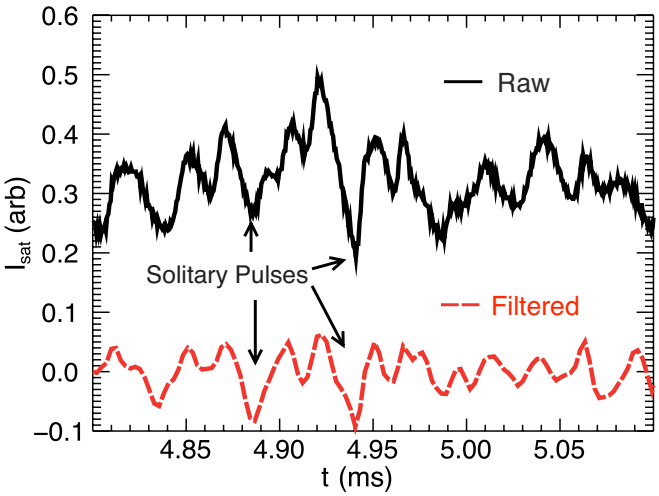

FIG. 12. (Color online) Single-shot time series of ion saturation current in temperature filament experiment. Solid black curve is raw signal containing features of coherent, low and high-frequency modes within which solitary pulses are embedded. Dashed red curve is the result of using FFT filtering that makes solitary pulses more evident, as indicated by the arrows.

spectrum having an exponential frequency dependence. Figure 12 illustrates pulses identified using a filtering method in which coherent peaks within the FFT are manually reduced to the background level. This reduces the amplitude of the coherent oscillations while leaving phase information intact. Filtering is used to identify pulses in the time series, but it is not a factor in the observation of exponential spectra. Reported spectra are calculated either without filtering or with low-pass filtering in which the cut-off frequency is above the highest frequency shown in the plot.

The pulses shown in Figs. 13 and 14 are obtained using a method that fits the data to a Lorentzian function similar to that of Eq. (2), except that in the fitting function the amplitude is not normalized. This allows for the amplitude of the measured pulse to vary. Operationally, a Lorentzian pulse of set width is slid through the time series and a fit is performed at each window corresponding to this width. The center of the fitting window is always redefined to time equal to zero so that the best fit across a measured pulse is obtained. Thresholds to define a successful fit are set manually after reviewing the results from an initial analysis. Once the limits on these quality factors (the standard deviation of the width and the convergence of the fit) are set, multiple analyses using different pulse widths are performed. In practice, due to the small variability of the measured widths of individual pulses it is usually sufficient to perform the fitting once. This is accomplished by using a width that is calculated from the slope of the ensemble averaged exponential spectra corresponding to the data set.

The existence of pulses with negative polarity in the ion

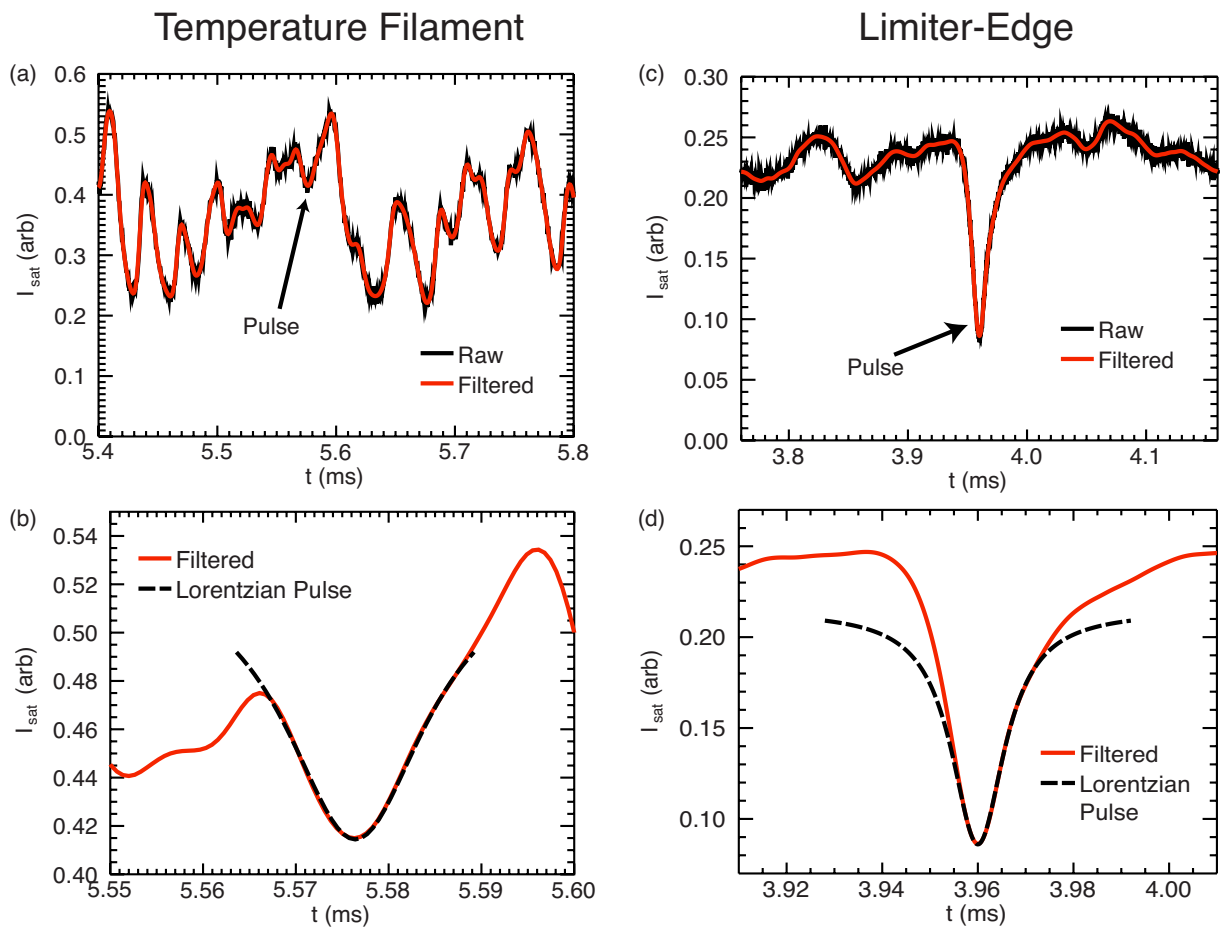

FIG. 13. (Color online) Examples of Lorentzian pulses displaying negative polarity for the temperature filament (left panels) and limiter-edge (right panels) experiments.

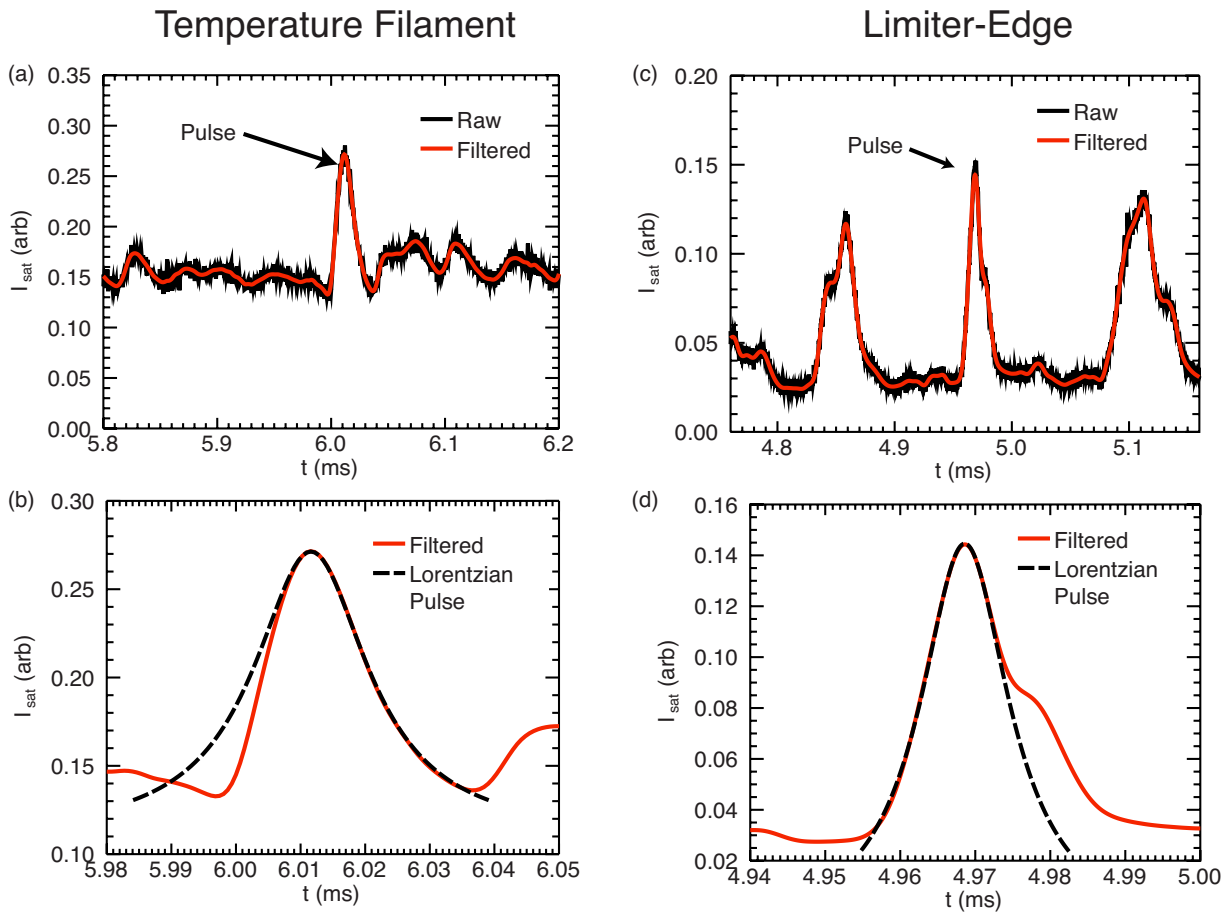

FIG. 14. (Color online) Examples of Lorentzian pulses displaying positive polarity for the temperature filament (left panels) and limiter-edge (right panels) experiments.

saturation current is demonstrated in Fig. 13 for the temperature filament (left panel) and the limiter-edge (right panel) experiments. The top graphs in the right and left panels show typical, single-shot time series for each experimental configuration. They correspond to measurements taken in the appropriate "center regions" delineated in Figs. 4 and 10. The "raw" signals are the black curves and the filtered signals are the red curves. The black arrow singles out an individual negative pulse that is displayed over an expanded time scale in the bottom graph of each panel. The temporal shape of the expanded, individual pulses is compared to a Lorentzian function [i.e., Eq. (2)] represented by the black dashed curve. It is seen that for both experiments a significant portion of the "pulse event" is well represented by the Lorentzian function. Some of the deviations from a pure Lorentzian shape arise because the pulses are embedded in a continuous stream of other fluctuations that are not filtered out completely. But there could be an additional distortion to the Lorentzian shape that is intrinsic to the process that generates the pulses. The sensitivity of the exponential spectrum to such distortions is examined in the next section.

Lorentzian pulses having positive polarity in the ion saturation current are also detected in both experiments, as shown in Fig. 14 in a format identical to that used in Fig. 13. It is of significance, however, that the spatial region in which the positive pulses are predominantly observed corresponds to the appropriate "outer regions" of the pressure profiles. In the limiter-edge environment the positive pulses have been related[27] to "blob phenomena,"[28–30,38–40] a topic of significant current interest in fusion studies.

Finally, it should be strongly emphasized that thousands of pulse events of the type illustrated in Figs. 13 and 14 have been identified in these investigations. The limiter-edge experiment corresponds to a steady-state pressure gradient in which pulses are observed. These pulses admit a viable statistical description, as shown in Fig. 4(a) of Ref. 27. The temperature filament experiment differs in that it features a three-dimensional structure whose parameters evolve in time. Consequently, an analogous statistical description is not useful.

VI. MODELING THE EXPONENTIAL SPECTRUM

While the power spectrum of a single Lorentzian pulse is exponential, it does not necessarily follow that the spectrum of a series of Lorentzian pulses is exponential. Consider a time signal composed of a sum of individual Lorentzian pulses,

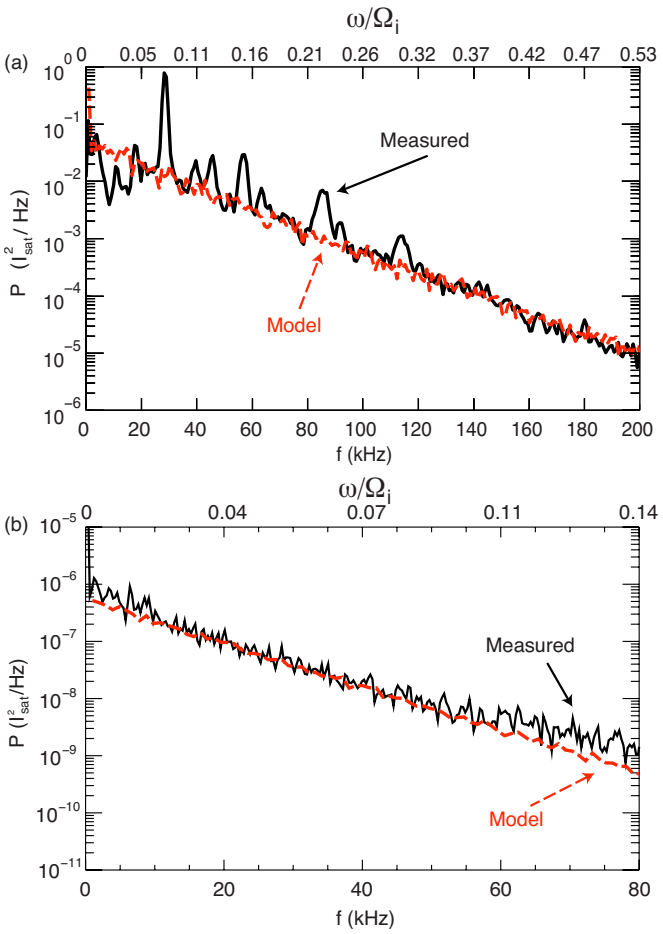

FIG. 15. (Color online) Modeling the ensemble-average power spectrum. Black curve is the measurement and dashed red curve is the prediction of a numerical model consisting of an ensemble of individual pulses having a Lorentzian temporal shape. (a) For the temperature filament experiment the model uses a width distribution between 2.5–4.5 μs. (b) For the limiter-edge experiment (the "outer" curve from Fig. 11) the model uses a width distribution between 6–8 μs.

$$p(t) = \sum_{i=0}^{N} L_i(t) = \sum_{i=0}^{N} \frac{A_i}{1 + [(t - t_{oi})/t_{ci}]^2}, \tag{4}$$

with different amplitudes, A_i, centered at different times, t_{oi}, and with different widths, t_{ci}.

The Fourier transform of $p(t)$ is

$$\tilde{p}(\omega) = \sum_{i=0}^{N} \pi A_i t_{ci} \exp(i\omega t_{oi}) \exp(-\omega t_{ci}), \tag{5}$$

a sum of exponential terms. It is not apparent that the logarithm of the power spectrum of $p(t)$, i.e., $\log[\tilde{p}(\omega)\tilde{p}^*(\omega)]$, can produce a linear function of angular frequency, ω. To explore this question it is helpful to turn to a numerical model.

Figure 15 compares an average power spectrum obtained from measurements in both experiments to model results. Figure 15(a) compares the average power spectrum obtained from temperature filament data to a power spectrum computed from an ensemble of model signals of the type expressed by Eq. (4). The model ensemble has 100 members. Each member is a time signal 1 ms in duration composed of the sum of ten Lorentzian pulses ($N=10$). Increasing the number of pulses results in an increased amplitude of the power spectra without affecting the spectral shape (i.e., the slope of the exponential is unchanged). The center times, t_{oi}, are randomly distributed over the 1 ms time interval and allow pulses to overlap. It is observed that pulse overlap, similar in degree to that measured in the experiments, does not affect the resulting exponential spectra. The amplitudes, A_i, are uniformly distributed over the range from 0.75 to 1.25, with the average amplitude being unity. The widths, t_{ci}, are uniformly distributed over the range between 2.5–4.5 μs. The average pulse width of the model ensemble, $t_c = \langle t_{ci} \rangle = 3.5$ μs, correctly represents the slope of the observed power spectrum, $f_s = 1/2\pi t_c$, for a power spectrum having the form $\exp(-2f/f_s)$. This average width for the model is calculated after matching the slope of the measured power spectrum. It is very close to the average width obtained from fitting an ensemble of measured individual pulses directly, $\langle t_{ci,\mathrm{exp}} \rangle = 4.0$ μs. Figure 15(b) shows the corresponding comparison between model and data for the limiter-edge experiment. The pulse widths of the model are uniformly distributed over the range 6–8 μs for this case, with an ensemble average of 7.0 μs. The measured pulses have an average width of 7.2 μs. Again, the frequency scale corresponding to the slope of the power spectrum agrees with the average width of the individual pulses.

It is appropriate to inquire how sensitive is the exponential power spectrum obtained from the model to the shape of individual pulses comprising the ensemble. After all, any symmetric pulse has a parabolic behavior near its peak value. Near the peak a Taylor series expansion of a temporal signal, $p(t)$, that represents a positive, symmetric pulse of unit amplitude, centered at $t=t_o$, gives $p(t) = 1 - (t - t_o)^2/t_c^2$, where the characteristic width of the pulse is $t_c = [\ddot{p}(t_o)/2]^{-1/2}$. What distinguishes one pulse shape from another? To investigate this question we consider the Fourier transforms of three basic pulse shapes: Lorentzian, Gaussian, and sech^2, all with the same characteristic width, t_c. A normalized Lorentzian pulse, $L(t)$, centered at $t=0$, has the shape

$$L(t) = \frac{t_c^2}{t^2 + t_c^2} = \frac{1}{1 + \bar{t}^2}, \tag{6}$$

where t_c is the pulse width, and $\bar{t} = t/t_c$ is the normalized time. A normalized Gaussian pulse, $G(t)$, centered at $t=0$, has the form

$$G(t) = \exp(-\bar{t}^2), \tag{7}$$

and a normalized sech^2 pulse, centered at $t=0$, has the form

$$S(t) = \frac{1}{\cosh^2(\bar{t})}. \tag{8}$$

The power spectrum of each basic pulse shape is presented in Fig. 16 in a semilog format. The characteristic width, t_c, of all three pulses is taken to be 3.5 μs in this example, i.e., the pulses have identical shapes near their peak values but their wings differ. In the semilog format, the power spectrum of the Lorentzian pulse is linear. The Gaussian pulse is never very close to a linear shape, and therefore

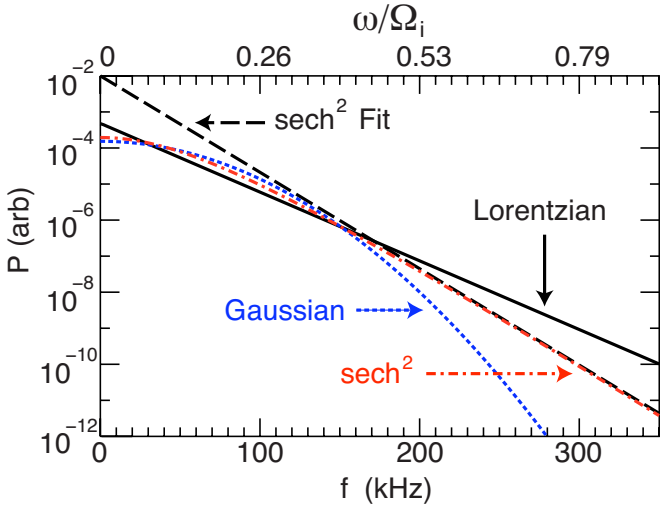

FIG. 16. (Color online) Semilog display of power spectra of three basic pulse shapes having identical parabolic approximations near their peak value. The normalized frequency (ω/Ω_i) is calculated using the parameters of the temperature filament experiment to provide a perspective. Only the Lorentzian pulse yields a linear behavior over the entire frequency range in this display. The dashed line is a fit to the linear part of the spectrum corresponding to the sech^2 pulse.

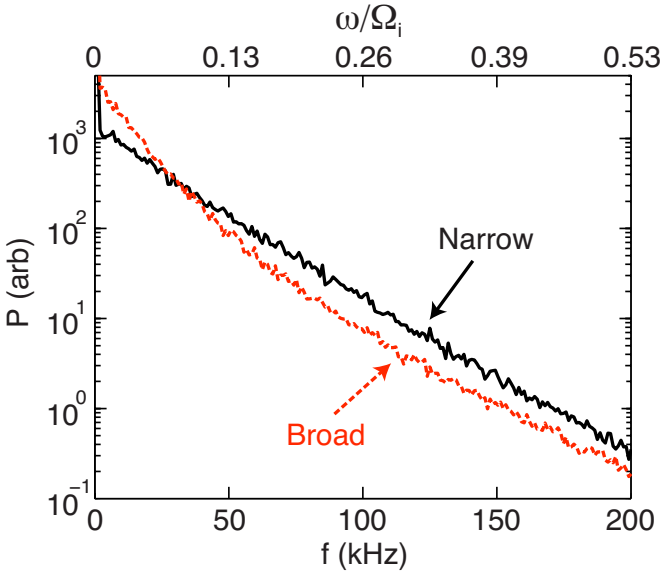

FIG. 17. (Color online) Power spectra of two ensembles of Lorentzian pulses with different distribution of widths. Solid black curve corresponds to a uniform width distribution between 2.5–4.5 μs, and the dotted red curve to the range 2.0–10.0 μs. The normalized frequency scale (ω/Ω_i) corresponds to the parameters of the temperature filament experiment.

is easy to distinguish from the Lorentzian. On the other hand, the power spectrum of the sech^2 pulse is very nearly linear at higher frequencies, and therefore could be difficult to distinguish from the Lorentzian pulse. However, the slope of the power spectrum corresponding to the sech^2 pulse is steeper than that for the Lorentzian pulse. Thus the characteristic spectral frequency corresponding to the sech^2 pulse is lower than that associated with the Lorentzian pulse.

In Fig. 16 the characteristic spectral frequency associated with the Lorentzian is $f_L=1/(2\pi t_c)=45.47$ kHz for $t_c=3.5$ μs. The curve $\exp(-2f/f_L)$ exactly matches the numerically generated power spectrum of the Lorentzian pulse. In contrast, the approximate exponential fit to the power spectrum of the sech^2 pulse, the dashed line in Fig. 16, yields $f_S=32.48$ kHz. This lower frequency corresponds to a Lorentzian pulse of characteristic time $t_c=4.9$ μs, which is inconsistent with the prescribed value $t_c=3.5$ μs. Thus, while the slope of the spectrum of the sech^2 pulse is linear in the upper frequency range, the characteristic time associated with the slope of the spectrum does not match the characteristic time of the pulse. The consistency between the characteristic slope of the semilog display of the power spectrum and the pulse width provides a means for distinguishing between these pulse shapes.

The power spectra of signals consisting of sums of individual Gaussian and sech^2 pulses can be obtained from ensembles constructed in the same manner as the Lorentzian model used to produce the results presented in Fig. 15. The result is that the ensemble average power spectra retain the same basic shape of the power spectra of the individual pulses. Thus the individual pulse shape determines the shape of the ensemble of pulses and this fact can be used to distinguish between pulse shapes. The Lorentzian pulse shape is essential to obtain an exponential power spectrum.

We also present an example for which an ensemble consisting of a sum of Lorentzian pulses does not result in a power spectrum linear in frequency. Figure 17 compares the power spectra of an ensemble of Lorentzian pulses with widths evenly distributed between 2.5–4.5 μs to an ensemble of Lorentzian pulses with widths evenly distributed over a much broader range between 2.0–10.0 μs. The wider distribution of pulse widths results in a power spectrum that noticeably departs from a linear shape at lower frequencies.

This example illustrates that the distribution of widths of Lorentzian pulses must be fairly narrow to result in the linear power spectra curves observed in the data.

Many examples of asymmetric pulses appear in the data of the two experiments reported here. It is also the case that previous studies of edge turbulence have reported[41,42] asymmetries in the temporal shape of "blobs." Consequently, it is natural to inquire about the effects of this asymmetry on the power spectrum. It is shown next that the modest asymmetries observed in the present experiments do not prevent the emergence of an exponential spectrum.

An example of an asymmetric pulse measured in the limiter-edge experiment (solid black curve), together with a numerical fit (dashed red curve), is given in Fig. 18(a). This pulse has been previously shown in the bottom right panel of Fig. 13. A much better fit to these asymmetric pulses can be obtained by multiplying the basic Lorentzian shape, $L(t)$, by a function of the form

$$f(t) = 1 + a(1 + b\{1 + \tanh[(t - t_1)/t_2]\}). \quad (9)$$

Figure 18(a) illustrates that a very close fit to the measured asymmetric pulse can be obtained using a product fitting function of the form $f(t)L(t)$. The asymmetry of the pulse shape introduced by a function of the type given in Eq. (9) has very little effect on the power spectrum, as illustrated in Fig. 18(b) which shows a comparison between the power

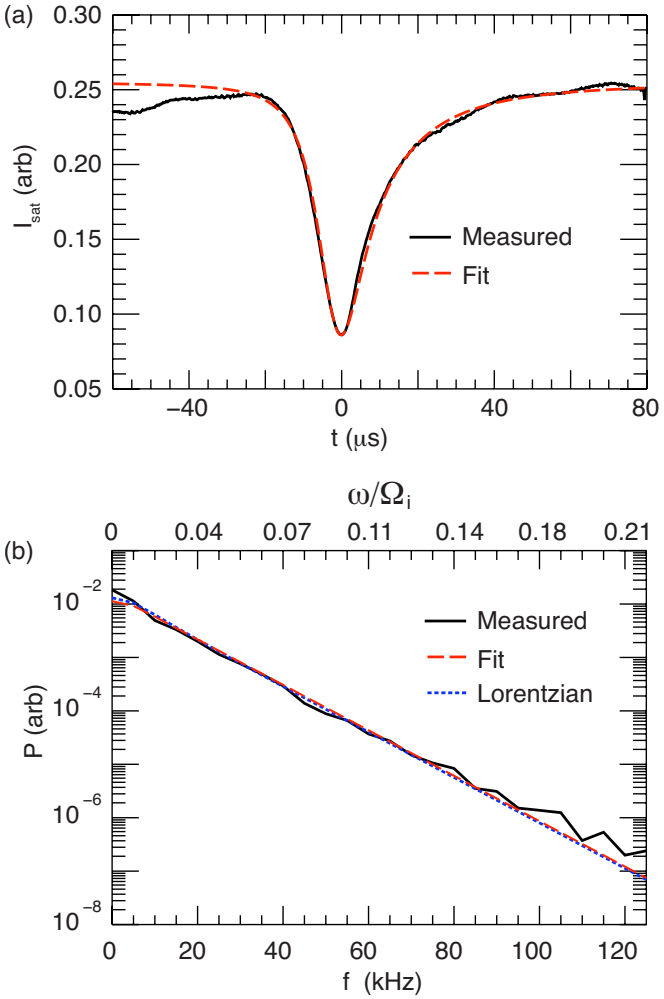

FIG. 18. (Color online) Effect of pulse asymmetry on the exponential spectrum. (a) Solid black curve is a measured pulse previously shown in the bottom right panel of Fig. 13. Dashed red curve is a functional fit consisting of a Lorentzian multiplied by a distortion given by Eq. (9). (b) Power spectra of the measured pulse (solid black) compared to that of the fit (dashed red) and of the fundamental Lorentzian pulse (dotted blue). The normalized frequency scale corresponds to the limiter-edge experiment in which the pulse is observed.

spectrum of the product fitting function, fL, the power spectrum of the basic Lorentzian, L, and the power spectrum of the individual pulse. The power spectrum of the Lorentzian [solid black line in Fig. 18(b)] and the skewed Lorentzian (dashed red line labeled "fit") are almost indistinguishable and both represent the power spectrum of the individual pulse very well, but for a slight deviation at higher frequencies. The exponential nature is retained over a broad frequency range. This example shows in detail that the asymmetry of pulses observed in the data does not destroy the exponential nature of the power spectrum.

While the particular example given here shows no discernible difference between the power spectrum of the basic Lorentzian fit and the product fitting function, the general case is that the power spectra of the two fits will differ. However, for the two experimental studies presented here, the differences are found to be small and occur at low frequencies (below 20 kHz). In general, observed asymmetries in individual pulse shape do not alter the exponential nature of the power spectrum.

VII. CONCLUSIONS

An extensive investigation has been made of the turbulent fluctuations in the frequency band below the ion cyclotron frequency in two different experiments involving pressure gradients across the confinement magnetic field in a large plasma column. One experiment involves a controlled, pure electron temperature gradient associated with a microscopic (6 mm gradient length) hot-electron temperature filament created by the injection of a small electron beam embedded in the center of a large, cold magnetized plasma. The other experiment is a macroscopic (3.5 cm gradient length) limiter-edge experiment in which a density gradient is established by inserting a metallic plate at the edge of the nominal plasma column of the LAPD-U.

The two different experiments are found to exhibit a broadband turbulence that displays an ensemble-averaged, exponential frequency spectrum for frequencies below the ion cyclotron frequency. By carefully examining the individual time series of the fluctuating quantities, at fixed spatial locations, the exponential feature has been traced, in both experiments, to the generation of pulses having a Lorentzian temporal signature.

Since the pressure gradient in the temperature filament experiment is determined by the application of a heat source under external control, this configuration provides unique insight into the phenomena. The temperature filament experiment permits the clear observation of the transition from a quiescent regime, regulated by classical heat transport, to a turbulent regime displaying broadband fluctuations and a concomitant departure from classical transport. The broadband is the consequence of pulses of Lorentzian temporal shape generated by nonlinear interactions of drift-Alfvén waves driven unstable by the pressure gradient. The temporal width of the pulses is measured to be a fraction of a period of the drift-Alfvén waves and sets the scaling frequency for the observed exponential spectrum.

The limiter-edge experiment also provides a unique element to the study. In this case there is no well-defined starting point and thus a transition from a quiescent to a turbulent regime is not observed. Here one encounters a steady-state, turbulent regime in which the Lorentzian pulses are copiously generated. They result in a pure exponential frequency spectrum, not mixed with coherent peaks, as is the case for the temperature filament. In spite of the intrinsically turbulent nature of the environment in this experiment, the distribution of the pulse widths of the Lorentzian pulses is very narrow, as is also the case in the temperature filament experiment.

A numerical model consisting of an ensemble of random Lorentzian pulses is found to reproduce the exponential spectrum observed in both experiments. Furthermore, the separate measurement of the average temporal-width of numerous pulses, identified from the time series, is found to be in close agreement with the pulse-width independently deter-

mined from the slope of the ensemble-average frequency spectrum, extracted from a semilog display.

A strong conclusion of the study is that an exponential frequency spectrum is a signature of Lorentzian pulses generated by drift-Alfvén waves. Because of the significant differences in the two situations investigated in detail (i.e., one is microscopic, the other macroscopic, one is a pure temperature gradient, the other is a density gradient, one is embedded in an essentially infinite plasma, the other is in contact with boundaries) this investigation strongly suggests that an exponential frequency spectrum is a universal feature of pressure-gradient driven turbulence in magnetized plasmas. The universality suggested by the present results may provide an explanation for previous observations in other magnetic confinement devices.

An open question that deserves close consideration, both experimental and theoretical, pertains to the spatial morphology that accompanies the temporal Lorentzian signature. Perhaps it is valuable to explore the observed deviations from pure Lorentzian shape to obtain deeper insight into the spatial structure. The present study has conclusively identified that temporal pulses of both polarities are generated. Positive pulses are predominantly found in the "outer region" of the pressure gradient while pulses with negative polarity are more frequently found in the "center" and "inner region." A cautionary statement must be made that no measurements have been performed that relate the two-polarity features simultaneously, nor any information is available about the extended spatial propagation of individual pulses. The techniques in the present investigation are unable to provide an answer to these issues. What is required is an instantaneous diagnostic that is able to image the complete fluctuation profile across the magnetic field without perturbing the system.

ACKNOWLEDGMENTS

D.C.P. and T.A.C. acknowledge support from NSF CAREER Grant No. PHY-0547572 and DOE Fusion Science Center Cooperative Agreement No. DE-FC02-04ER54785. J.E.M. and G.J.M.'s work was performed under the auspices of the BaPSF, which is jointly supported by a DOE-NSF cooperative agreement.

[1] J. A. Krommes, Phys. Rep. **360**, 1 (2002).
[2] W. Horton, Rev. Mod. Phys. **71**, 735 (1999).
[3] Committee on Solar and Space Physics, *Plasma Physics of the Local Cosmos* (National Academies, Washington, D.C., 2004).
[4] F. F. Chen, Phys. Rev. Lett. **15**, 381 (1965).
[5] K. Kamataki, Y. Nagashima, S. Shinohara, Y. Kawai, M. Yagi, K. Itoh, and S.-I. Itoh, J. Phys. Soc. Jpn. **76**, 054501 (2007).
[6] B. Labit, A. Diallo, A. Fasoli, I. Furno, D. Iraji, S. H. Müller, G. Plyushchev, M. Podestà, F. M. Poli, P. Ricci, C. Theiler, and J. Horacek, Plasma Phys. Controlled Fusion **49**, B281 (2007).
[7] M.Škori ć and M. Rajković, Contrib. Plasma Phys. **48**, 37 (2008).
[8] V. P. Budaev, S. Masuzaki, T. Morisaki, N. Ohno, N. Asakura, S. Takamura, H. Yamada, and A. Komori, J. Plasma Fusion Res. **3**, S1019 (2008).
[9] M. A. Pedrosa, C. Hidalgo, B. A. Carreras, R. Balbín, I. García-Cortés, D. Newman, B. van Milligen, E. Sánchez, J. Bleuel, M. Endler, S. Davies, and G. F. Matthews, Phys. Rev. Lett. **82**, 3621 (1999).
[10] U. Stroth, F. Greiner, C. Lechte, N. Mahdizadeh, K. Rahbarnia, and M. Ramisch, AIP Conf. Proc. **11**, 2558 (2004).
[11] B. A. Carreras, R. Balbin, B. van Milligen, M. A. Pedrosa, I. Garcia-Cortes, E. Sanchez, C. Hidalgo, J. Bleuel, M. Endler, H. Thomsen, A. Chankin, S. Davies, K. Erents, and G. F. Matthews, Phys. Plasmas **6**, 4615 (1999).
[12] S. J. Zweben, J. A. Boedo, O. Grulke, C. Hidalgo, B. LaBombard, R. J. Maqueda, P. Scarin, and J. L. Terry, Plasma Phys. Controlled Fusion **49**, S1 (2007).
[13] C. M. Tchen, Plasma Phys. **15**, 1193 (1973).
[14] F. S. Kuo and S. Y. Chou, Chin. J. Physiol. **39**, 577 (2001).
[15] L. J. Milano, S. Dasso, W. H. Matthaeus, and C. W. Smith, Phys. Rev. Lett. **93**, 155005 (2004).
[16] G. Zimbardo, Plasma Phys. Controlled Fusion **48**, B295 (2006).
[17] S. D. Bale, P. J. Kellogg, F. S. Mozer, T. S. Horbury, and H. Reme, Phys. Rev. Lett. **94**, 215002 (2005).
[18] A. Kolmogorov, Dokl. Akad. Nauk SSSR **32**, 16 (1941); [reprinted in Proc. R. Soc. London **434**, 15 (1991)].
[19] U. Frisch, *Turbulence: The Legacy of A. N. Kolmogorov* (Cambridge University Press, Cambridge, 1995).
[20] D. C. Pace, M. Shi, J. E. Maggs, G. J. Morales, and T. A. Carter, Phys. Rev. Lett. **101**, 085001 (2008).
[21] W. Gekelman, H. Pfister, Z. Lucky, J. Bamber, D. Leneman, and J. Maggs, Rev. Sci. Instrum. **62**, 2875 (1991).
[22] H. Xia and M. G. Shats, Phys. Rev. Lett. **91**, 155001 (2003).
[23] G. Fiksel, S. C. Prager, P. Pribyl, R. J. Taylor, and G. R. Tynan, Phys. Rev. Lett. **75**, 3866 (1995).
[24] U. Kauschke, G. Oelerich-Hill, and A. Piel, Phys. Fluids B **2**, 38 (1990).
[25] J. E. Maggs and G. J. Morales, Phys. Plasmas **10**, 2267 (2003).
[26] S. J. Zweben, Phys. Fluids **28**, 974 (1985).
[27] T. A. Carter, Phys. Plasmas **13**, 010701 (2006).
[28] G. Y. Antar, Contrib. Plasma Phys. **44**, 217 (2004).
[29] I. Furno, B. Labit, M. Podestà, A. Fasoli, S. H. Müller, F. M. Poli, P. Ricci, C. Theiler, S. Brunner, A. Diallo, and J. Graves, Phys. Rev. Lett. **100**, 055004 (2008).
[30] D. A. D'Ippolito, J. R. Myra, and S. I. Krasheninnikov, Phys. Plasmas **9**, 222 (2002).
[31] A. T. Burke, J. E. Maggs, and G. J. Morales, Phys. Plasmas **7**, 544 (2000).
[32] S. I. Braginskii, in *Reviews of Plasma Physics*, edited by M. A. Leontovich (Consultants Bureau, New York, 1965), Vol. 1, p. 205.
[33] L. Spitzer and R. Härm, Phys. Rev. **89**, 977 (1953).
[34] A. T. Burke, J. E. Maggs, and G. J. Morales, Phys. Rev. Lett. **81**, 3659 (1998).
[35] J. R. Peñano, G. J. Morales, and J. E. Maggs, Phys. Plasmas **7**, 144 (2000).
[36] A. T. Burke, J. E. Maggs, and G. J. Morales, Phys. Plasmas **7**, 1397 (2000).
[37] D. C. Pace, M. Shi, J. E. Maggs, G. J. Morales, and T. A. Carter, Phys. Rev. Lett. **101**, 035003 (2008).
[38] A. Fredriksen, C. Riccardi, L. Cartegni, and H. Pecseli, Plasma Phys. Controlled Fusion **45**, 721 (2003).
[39] B. A. Carreras, J. Nucl. Mater. **337–339**, 315 (2005).
[40] C. Hidalgo, B. P. van Milligen, and M. A. Pedrosa, C. R. Phys. **7**, 679 (2006).
[41] G. Y. Antar, G. Counsell, Y. Yu, B. Labombard, and P. Devynck, Phys. Plasmas **10**, 419 (2003).
[42] J. A. Boedo, D. Rudakov, R. Moyer, S. Krasheninnikov, D. Whyte, G. McKee, G. Tynan, M. Schaffer, P. Stangeby, P. West, S. Allen, T. Evans, R. Fonck, E. Hollmann, A. Leonard, A. Mahdavi, G. Porter, M. Tillack, and G. Antar, Phys. Plasmas **8**, 4826 (2001).